## P3.2 BARRIER JETS IN THE GULF OF ALASKA - A SATELLITE CLIMATOLOGY

Kenneth Loescher [1], George Young [1 *], Nathaniel Winstead [2], Brian Colle [3]
[1] The Pennsylvania State University, University Park, Pennsylvania, [2] Johns Hopkins University Applied Research Laboratory, Columbia, Maryland, [3] State University of New York - Stony Brook, Stony Brook, New York

### 1. INTRODUCTION

Strong mountain-parallel, low-level mesoscale wind maxima, commonly referred to as barrier jets, are often observed along the synoptically windward slopes of mountain ranges. Barrier jets are routinely observed in cases of cold air damming along the east coast of the United States (Bosart and Bell 1988) and have also been observed in Taiwan (Li and Chen 1998), the western slopes of the Sierra Nevada (Parish 1982; Marwitz 1987), the Front Range of the Colorado Rockies (Marwitz and Toth 1993), Antarctica (Schwerdtfeger 1975), the west coast of the United States (Doyle 1997), and Alaska (Schwerdtfeger 1974; Overland and Bond 1993).

Barrier jets form as a result of the interaction of synoptic-scale flow with mountainous terrain (Schwerdtfeger 1974). Flow encountering elevated terrain undergoes forced ascent causing the kinetic energy associated with the barrier normal flow to be converted into potential energy. If the magnitude of the barrier-normal flow decreases to zero below the crest of the terrain, the flow is blocked from passing over the mountain. It is this blocking that sets the stage for barrier jet formation (Schwerdtfeger 1974).

Deceleration in the barrier normal direction disrupts the balance of forces, allowing the synoptic-scale pressure gradient force to dominate. This imbalance leads to a leftward (Northern Hemisphere) deflection of the wind direction, and subsequent acceleration of the flow down the synoptic pressure gradient. After the flow has become barrier parallel, the Coriolis force is directed normal to and toward the barrier acting to drive the flow against the side of the mountain barrier. The resulting mass accumulation along the upwind slope of the barrier produces a mesoscale pressure ridge. If the blocking persists, balance is eventually reached between this induced pressure gradient force and the Coriolis force resulting in barrier parallel flow. Barrier-parallel acceleration continues until antitriptic balance is achieved in the along-mountain direction (Bosart and Bell 1988). The final three-way force balance often leads to significant low-level wind speeds parallel to the mountain.

The upslope flow required for barrier jet formation can be provided by sources other than synoptic-scale wind systems. When a significant pressure difference exists between opposing sides of a mountain range, air from the high-pressure side is frequently drawn through the gaps in the mountain range. Upon exiting the gap, this unbalanced flow can be turned by the Coriolis force to become mountain-parallel, or even acquire a component toward the barrier. In the latter case, the flow is susceptible to blocking, and barrier jet formation can occur. Barrier jets that originate from gap flow will be referred to as hybrid jets. A visual depiction of both barrier jet and hybrid jet formation can be seen in Fig. 1.

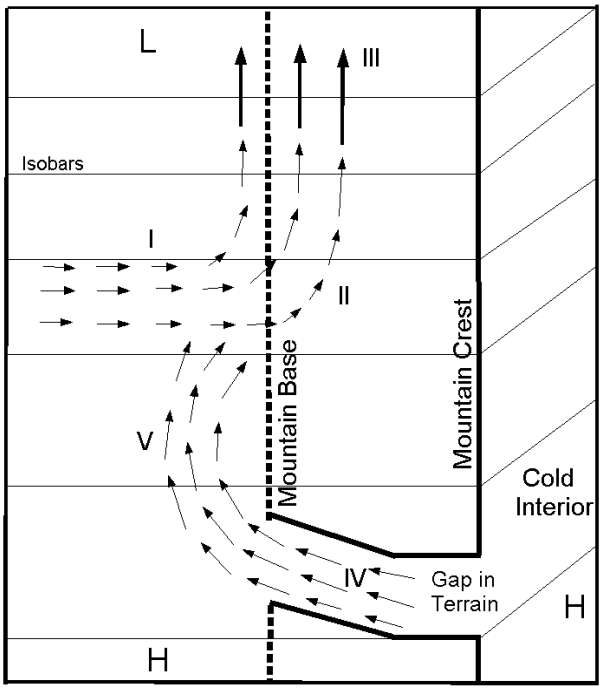


*Figure 1. Visual depiction of barrier and hybrid jet formation. For barrier jets, onshore flow (I), begins to upslope and decelerate causing a leftward turn (II). This allows the parcel to accelerate down the pressure gradient and reach high speeds directed parallel to the mountain (III). Hybrid jets arise from gap flow (IV), which is turned after exiting the gap by Coriolis and pressure gradient forces (V). The flow is turned to an onshore direction, and can be blocked leading to hybrid jet formation.*

In order to quantify the likelihood of flow blocking and subsequent barrier jet formation, a parameter that accounts for the physics of the flow blocking is needed.

* Corresponding author address: George S. Young, 503 Walker Building, Dept. of Meteorology, The Pennsylvania State University, University Park, PA 16802

In its simplest form, $Fr = \frac{u}{h_m N}$, the Froude number is a measure of the amount of kinetic energy possessed by the barrier normal flow component prior to ascent compared to the amount of energy that would be required to lift that flow to the crest of the mountain. If Fr > 1 the flow is said to be supercritical and has enough energy to pass over the barrier. Flows with Fr < 1, are said to be subcritical and do not possess sufficient energy to cross the barrier. Fr depends on the ambient barrier normal velocity component ($u$), the height of the barrier ($h_m$), and the static stability parameter ($N$), where $N = \left[ \left( g / \overline{\theta} \right) \partial \theta / \partial z \right]^{1/2}$, $g$ is gravity, and $\overline{\theta}$ is the mean potential temperature.

This definition of Froude number assumes that rising air parcels cool at the dry adiabatic lapse rate. This assumption is often invalid, especially in coastal regions where moisture is abundant. If condensation occurs during ascent, the buoyancy of the parcel would increase which may allow otherwise sub-critical flows to pass over the barrier. For this reason, strong blocking is typically observed only when Fr << 1 (Pierrehumbert and Wyman 1985). While the Froude number can be corrected for this latent heating effect issues of surface moisture fluxes, precipitation evaporation, and glaciation must be dealt with for which data are not generally available, hence the dry adiabatic Froude number is typically used with the caveats discussed above (Bosart and Bell 1988).

Although the physics of barrier jet formation are quantified by the Froude number, it has been suggested that their width is controlled by the Rossby radius of deformation. For cases of steep orography, the distance upstream that the flow begins to decelerate is given by the radius of deformation ($l_R$), where $l_R = N h_m / f$ (Chen and Smith 1987), and $f$ is the Coriolis parameter. The orography is considered steep if the non-dimensional slope, $\left( h_m / l_m \right)(N / f) > 1$, where $l_m$ is the half-width of the mountain (Burger 1991). Thus, the horizontal extent of blocking depends on the stability, the height of the mountain, and the effect of the Earth's rotation.

The Alaskan coastline bordering the Gulf of Alaska has numerous topographic barriers in close proximity to the coast (Fig. 2) that are known to produce barrier jets (Overland and Bond 1993). The closeness of the mountains to the coast allows many of the barrier jets to extend over the water as will be shown below. These strong coastal wind events can be treacherous to the aviation and fishing industries in the region. For example, Overland and Bond (1993) state that motivation for their article came from a letter written by an angry fisherman who was caught in a poorly forecasted barrier jet near Yakutat in 1979.

This paper presents a five-year study from May 1998 through April 2003 of coastal barrier and hybrid jet occurrence in the Gulf of Alaska. Temporal and spatial distributions of barrier jet and hybrid occurrence highlight the favored seasons and locations for jet formation and explanations for shape of each distribution are given. The climatological values of structural characteristics of barrier and hybrid jets including strength, enhancement, width, and detachment, which are defined below, are also computed.

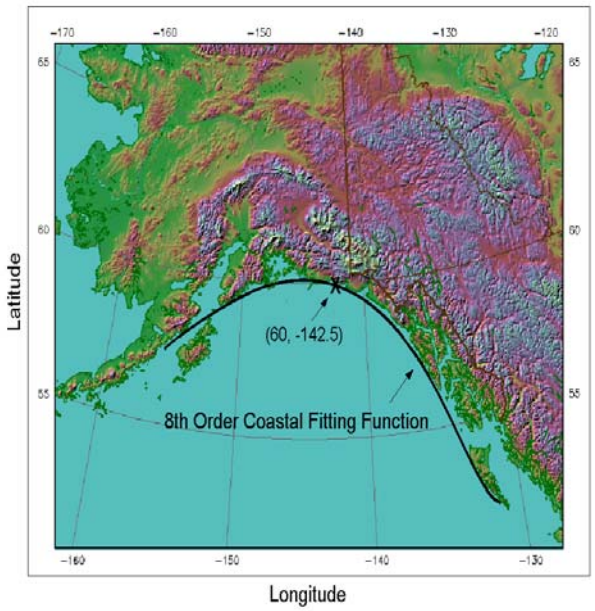


*Figure 2. Topographical map of Alaska with coastal fitting function (solid line), and location used for stability and wind analysis (X).*

## 2. DATA ANALYSIS AND PROCEDURES

Because this study focuses on coastal barrier and hybrid jets, spaceborne synthetic aperture radar (SAR) was the ideal choice for collecting surface wind speed observations. In situ observations are sparse in the study region with few observing stations located along the Alaskan coast, and even fewer observations available over the water. The data from these in situ observations is insufficient to resolve mesoscale barrier jets along the entire coastline. SAR wind mapping on the other hand, operates exclusively over the water, and provides sub-kilometer resolution coverage over a very large area. This combination of fine-scale resolution and mesoscale coverage is crucial for this study because of the small spatial scale of barrier jets and the large extent of the coast to be covered.

SAR wind mapping is possible because SAR backscatter derives from the short-wavelength sea surface roughness that results from the surface wind stress. Using a CMOD-like algorithm (Li et. al. 1999), the wind speed is inferred from the radar backscatter. Converting the backscatter field to wind speed does,

however, require knowledge of the wind direction. The required wind directions were obtained from NOGAPS model analyses.

For this study SAR wind speed data from the Canadian Radarsat-1 satellite (Radarsat) was used. The satellite data used were collected in wide-swath mode yielding 450 km wide spatial coverage and 100-200 m resolution (Pichel and Clemente-Colon 2000). A collection of all the SAR images of the Gulf of Alaska from May 1, 1998 to April 30, 2003 was obtained from the John's Hopkins University Applied Physics Lab (http://fermi.jhuapl.edu/people/winstead/web_wind_NSF/index.html). This collection included roughly 3000 images over the five-year study period.

Using SAR data for a study of this sort is not without its disadvantages. One major shortcoming of SAR is that only surface wind speeds can be obtained; thus, little insight is available about wind speeds or directions above the surface. Moreover, at low wind speeds SAR data can be contaminated with oceanographic events. This low wind speed contamination problem does not affect the current study to a large degree as barrier and hybrid jets are high wind events. A more crucial disadvantage for this study is that the ability of the CMOD4 algorithm to convert backscatter to wind speed at speeds much greater than 20 m $s^{-1}$ is questionable (Monaldo 2000). For this reason, the SAR wind speeds only go up to 25 m $s^{-1}$ in the available images. Thus, for the intense barrier and hybrid jets, a true maximum wind speed cannot be obtained using SAR. Another disadvantage of using SAR is that the wind direction field must be obtained from an external analysis as discussed above. Because the NOGAPS model is not perfect, there will inherently be some error in the SAR derived wind speeds.

The data used in presenting climatological values of stability, wind speed, wind direction, pressure, and temperature was obtained from the Climate Diagnostics Center in Boulder, Colorado (http://www.cdc.noaa.gov/cdc/data.ncep.reanalysis.html). The data are four time daily NCAR/NCEP reanalyses with a meridional and zonal grid spacing of 2.5°. Only three vertical layers exist from the surface to 2000m, a typical crest level along the coastal mountains. Data of such a low resolution yield information about the synoptic scale features that are important in barrier and hybrid jet formation, but cannot be used to verify the existence of barrier jets.

In order to produce a meaningful event climatology, the event criteria must be unambiguously defined. The criteria used in this study are as follows. A barrier jet is defined as a barrier-parallel wind maximum that is not a land-falling synoptic-scale front and is longer in the along-shore direction than the cross-shore direction. The maximum wind speed must be at least 1.5 times greater than the ambient onshore-directed flow, where the ambient flow is defined as the average flow found in close proximity (10 to 20 km) to the barrier jet. The edge of the barrier jet is defined as being along the isotach at 1.25 times this ambient synoptic flow. Hybrid jets are defined using the same criteria as barrier jets but must originate via offshore-directed gap flow that turns and becomes onshore. The terms used to describe the structure of barrier and hybrid jets follow. *Strength* is defined as the maximum wind speed observed at any point within the jet. *Width* is defined as the average distance from the edge of the topography deemed to be responsible for the barrier jet to the outer edge of the jet.

Obtaining a meaningful spatial distribution of barrier and hybrid jet occurrence required approximating the fractal coastline with a smooth curve, in this case an 8$^{th}$ order polynomial function relating latitude to longitude (Fig. 2). Sixty-two data points lying just offshore were used to generate the function. The function was then divided into 405 segments measuring 5 km each giving a total function length of 2025 km. The starting and ending points of the function are located at latitude and longitude 57.28N, 156.25W and 51.92N, 131.41W, respectively. A large majority of the points along the function lie approximately 10 km offshore, however, a few points lie a few km inland.

## 3. BARRIER JET DISTRIBUTIONS

The number of barrier jets observed in each month during the five year study period was calculated and the results were used to compute the temporal distribution of barrier jet occurrence which was then scaled to correct for the unequal satellite coverage. The scaled barrier jet distribution (Fig. 3) reflects the distribution of barrier jets by month that would be expected if each month had received equal satellite coverage and each month was 30 days in length. SAR imagery is not available for each point along the coast for all times in the study, so only the relative shape of the distribution has significance. It is not possible to state the exact number of barrier jets that occurred in each month with the data available.

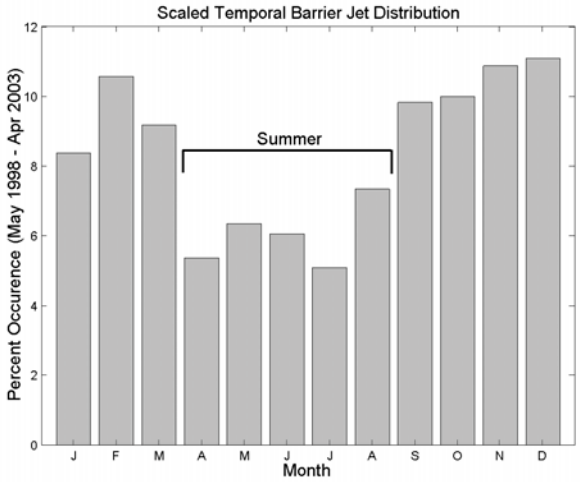


*Figure 3. Percent of all barrier jet cases by month after scaling to correct for unequal satellite coverage.*

It is clear from the scaled barrier jet distribution (Fig. 3) that barrier jets are more common during the

winter months (Sep.– Mar. is considered winter). After accounting for the unequal lengths of winter and summer, the winter months display a 65% higher likelihood of barrier jet occurrence for any given day. In fact the barrier jet frequency in December is nearly twice that in July.

Neglecting condensation, barrier jet formation depends on thee main factors: wind direction, stability, and barrier-normal velocity. Because the winter months produce a much higher percentage of the barrier jets than summer, it is logical to examine the seasonal differences for the three factors listed above.

All seasonal comparisons will be done for a single point located at 60N 142.5W (Fig. 2). This point lies just offshore and very near the Valdez-Cordova Mountains which produce the greatest number of barrier jets. For this particular mountain range, which faces nearly due south, favorable flow directions range from 120° to 180°. Twenty-six percent of the observations in the winter months had favorable flow directions, and 21% of the observations in the summer months had favorable directions. Thus, according to wind direction alone, winter months have a higher likelihood of barrier jet formation.

Using only those observations that had the correct flow direction, the effect of stability and barrier-normal wind speed on barrier jet formation can be examined. A combination of high stability and low wind speed would maximize the likelihood of barrier jet formation according to the Froude number. Bivariate distributions of barrier-normal wind speed versus stability (in the surface-925 mb layer) were created for both winter and summer and were normalized to account for the unequal lengths of winter and summer. The summer distribution of speed and stability was subtracted from the winter distribution to produce a distribution that reflects the relative likelihood of a speed and stability combination occurring in winter versus summer.

The resulting distribution (not shown) suggests that many more of the high-stability, weak-flow cases are found during the summer months. Because weak flow and high stability would favor flow blocking, it can be inferred that the summer months should experience a greater number of barrier jets. This was not observed however. It is possible that the choice of only classifying cases that had enhancement of 1.5 times the synoptic flow as barrier jets eliminated many weak barrier jets that occurred during the summer. A weak barrier-normal synoptic flow, which is more common in the summer, implies a weak pressure barrier-parallel gradient and therefore small accelerations in the barrier-parallel direction after blocking occurs. The winter months tend to produce more observations with high stability and high wind speeds. Any blocking of these cases would lead to strong barrier jets, which as will be shown below tend to occur almost exclusively in the winter months. Thus, in our definition of what we would classify as a barrier jet, we may have captured the distribution of stronger jets better than weaker jets.

Moisture effects must be considered as well when explaining the frequency of barrier jets between winter and summer. Mean lifting condensation level (LCL) heights were calculated for winter, summer, and barrier jet cases. Winter had a mean LCL of 90 m and the mean summer value was 134 m. The mean barrier jet LCL was found to be 100 m. The lower LCL height in winter means that rising parcels in the winter will cool moist adiabatically for greater vertical distances than parcels in the summer. The difference is small, however, when compared to the terrain crest level of 2000 m in this region. Because both winter and summer have similar LCL heights, it is reasonable to compare the amount of water vapor in the air during the two seasons (Fig. 4). Figure 4 shows markedly more water vapor during the summer months. Thus, one would expect more latent heat release and increased buoyancy in the rising parcels during the summer months vs. the winter months. Thus, the increased water vapor content may help to explain why more barrier jets are found during the winter months.

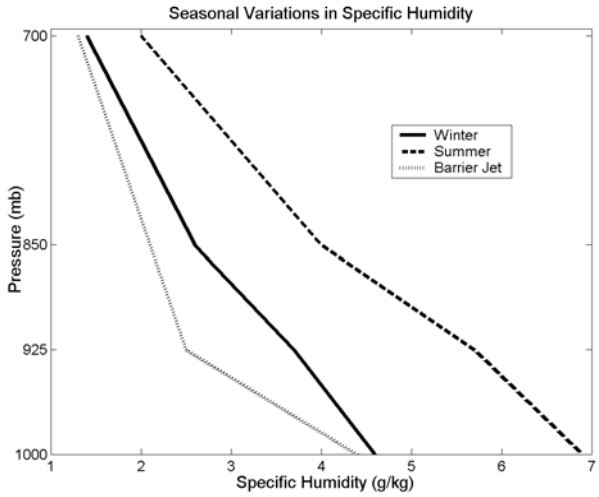


*Figure 4. Specific humidity for winter, summer and barrier jet cases at 60N, 142.5W. Only observations with favorable flow directions for barrier jet formation are included.*

To produce a spatial barrier jet climatology, the distance from the starting and ending point of a barrier jet to each point along the coastal function was calculated. The point on the function that was closest to the starting point of the barrier jet was considered to be the starting point of the jet on the function. The endpoint of the barrier jet on the function was found in the same manner. All the points on the function that lie between the starting and ending point were deemed to lie within the span of the barrier jet. A running total was kept of the number of barrier jets that were found at each point. The final tally of barrier jet occurrence at each point was then used to create the spatial barrier jet distribution.

As with the temporal distribution, the spatial distribution required scaling to account for unequal SAR coverage. Figure 5 shows the scaled distribution of barrier jets as a function of distance along the coastal

function. The spatial distribution reflects all barrier jet cases regardless of the month in which they occurred. The data can also be broken down into seasonal distributions (not shown). While there are far fewer barrier jets in the summer months, the shape of the distribution is similar in the two seasons.

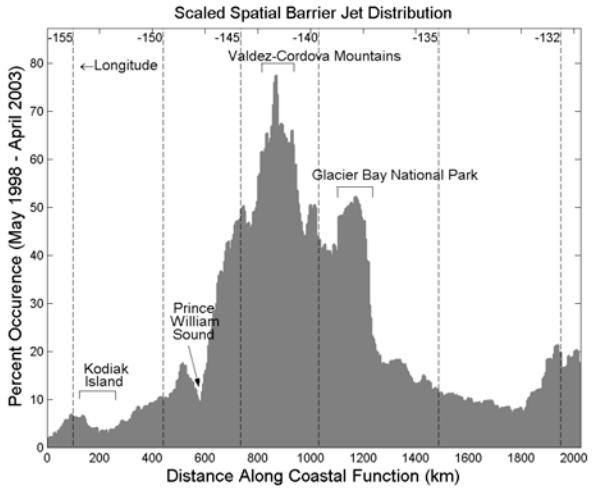


*Figure 5. Barrier jet distribution by distance along coastal function after accounting for unequal SAR coverage.*

Comparison of the total distribution shown in Fig. 5 to near-coast terrain height (e.g. Figs. 2 and 6) helps to qualitatively explain why certain areas are favored for barrier jet formation. The main peak in the barrier jet distribution is found alongside the Valdez-Cordova Mountains. This mountain range lies very near the coast and just to the west of Icy Bay. The second largest peak is adjacent to the near-coast mountains located in Glacier Bay National Park.

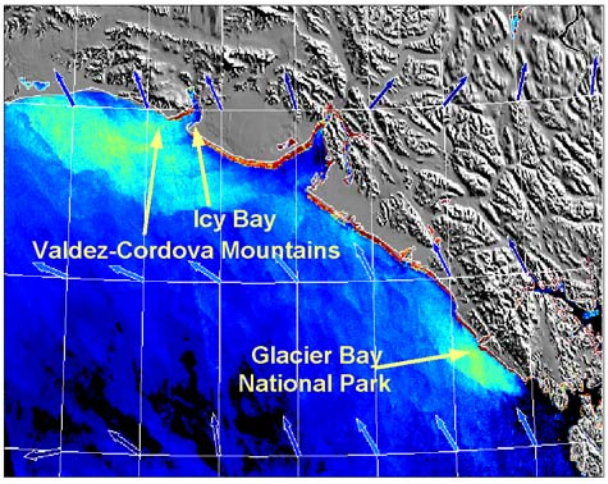


*Figure 6. SAR image of barrier jets resulting from near-coast high terrain.*

A terrain analysis was done along the entire coastal function to quantify the terrain effects on the barrier jet spatial distribution. At each point on the coastal function that was within 50 km of land (points that lie near straits and large bays were not included due to their large distances from land), a line orthogonal to the function at that point was directed inland, and terrain height values were recorded along the entirety of the line. Beginning where the terrain line first encountered land, the maximum terrain height found in the first 5 km inland was obtained. A distribution of these maximum terrain heights was produced along the entire coastal function. Analyses were also run for 10, 15, 20, 25, 30, 50, and 100 km windows. The general shape of the 100 km terrain profile matches the barrier jet distribution much more closely than that for the other windows. This suggests that terrain features on the order of 100 km (not shown) inland or more are important in barrier jet formation. The average terrain height in each of the windows was also calculated, but the resulting distributions did not fit the barrier jet distributions as well as the maximum terrain height windows did. Thus, profile terrain appears to be more relevant than average terrain, at least for these jagged mountain ranges.

A comparison of stabilities between days when barrier jets were observed and days when barrier jets were not observed provides some insight into the effect of the elevated stability previously mentioned. Figure 7 shows the difference in mean stability in the 925-850 mb layer between barrier jet days and non-jet days. This layer was chosen to reflect the existence of a stable lid below crest height. A wide area along the eastern coast of the Gulf of Alaska extending northward past Yakutat, was found to have higher stability during barrier jet events than during non-events (a two-sided *Student t* test with independent variances was used to determine the region of 95% confidence). The region where the higher stability is found corresponds to roughly the same region where the maximum number of barrier jets are located. The same comparison between barrier jet event stability and non-jet stability was done for the surface-850 mb layer, and the area with greater stability in the surface-based layer was much less extensive, and located farther offshore.

Twenty-six percent of all REANALYSIS observations were from 120-180°, which is the favorable flow direction for barrier jet formation. For the observations that were associated with barrier jet formation 63% had a wind direction from 110-180°. The same trend was observed at the 925 mb level, with a higher percentage of flows having a favorable orientation when barrier jets were observed.

It appears that several factors are involved in determining the temporal and spatial variations in barrier jet distribution. The occurrence of favorable wind direction, the strength of stability, and magnitude of the barrier-normal wind velocity alone do not fully explain the seasonal variations in barrier jet distributions. It is likely that moisture must be taken into account to resolve the inconsistencies of theory with the observations. The terrain height, the locations of

regions of elevated stability, and the open ocean wind direction relative to the coast, all appear to have a large impact on the favorable locations for barrier jet formation.

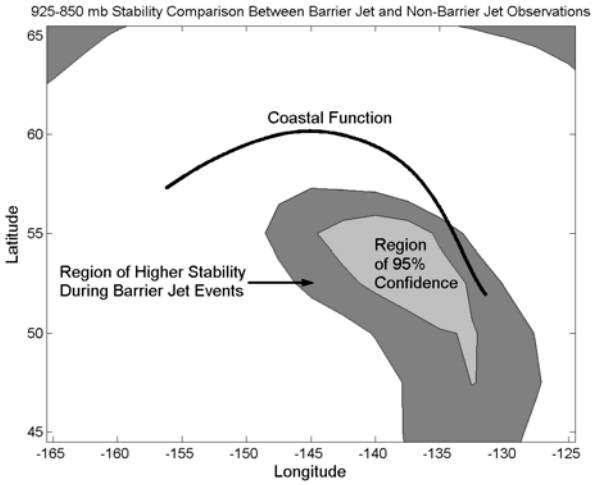


*Figure 7. Dark shaded region highlights locations where stability was found to be higher during barrier jet events. Lighter shaded regions denote areas where the calculated higher stability passes at the 95% confidence level on a double-sided Student t-test.*

## 4. HYBRID JET DISTRIBUTIONS

Temporal and spatial hybrid jet distributions for the five year period were created using the same procedures described for the barrier jets including scaling to correct for unequal SAR coverage. The scaled hybrid temporal distribution (Fig. 8) shows that hybrid formation is much more likely during the cold season. Very few hybrids were observed during June and July while December produced the maximum number of hybrids.

Considering that hybrids are defined as originating from offshore-directed gap flow, it is not surprising that hybrids are common during the winter months. The large cross-barrier pressure gradients that give rise to gap flow (Fig. 9a,b) are more common in the winter months (Fig. 9c,d) as a result of the large temperature difference between the cold interior and the relatively warm ocean. It follows then, that with a higher occurrence of gap flow, there is a higher likelihood that a hybrid will be formed. In addition, the blocking of any gap flow that is turned onshore may be enhanced during winter because the gap flow from the continental interior is typically much colder than the marine air it is displacing, leading to a much higher low-level stability profile during the winter events

The scaled hybrid spatial distribution is shown in Fig. 10a. The hybrid distribution has many more peaks than the corresponding barrier jet distribution (Fig. 5). Each distinct peak in the hybrid distribution is adjacent to a gap in the near-coast terrain. Figure 10 suggests that gap flows exiting Cross Sound, Yakutat Bay, and Icy Bay produce the most hybrids along the coast. The effectiveness of these gaps most likely results from their location immediately to the right of major mountains when viewed from offshore. For this configuration gap flow that is turned onshore has a high likelihood of encountering terrain high enough to induce blocking. The starting points of the hybrids, which are defined as the locations where the gap flows exit the gaps prior to hybrid jet formation, are shown in Fig.10b. The same five gaps that are implicated in Fig.10a are seen to in fact be the major hybrid producers, with Yakutat Bay being the most profligate.

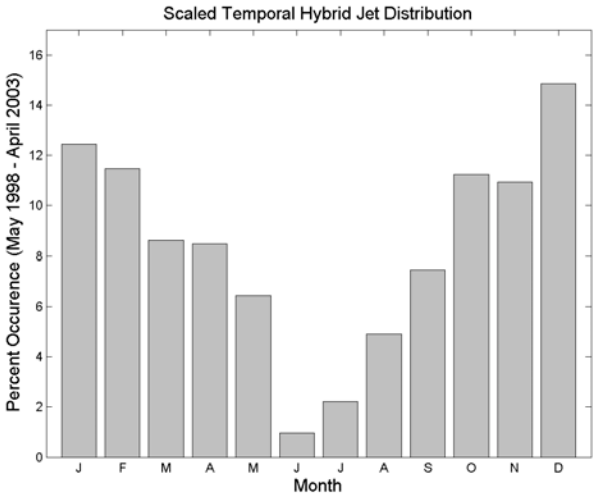


*Figure 8. Hybrid jet distribution by month after correcting for unequal SAR coverage.*

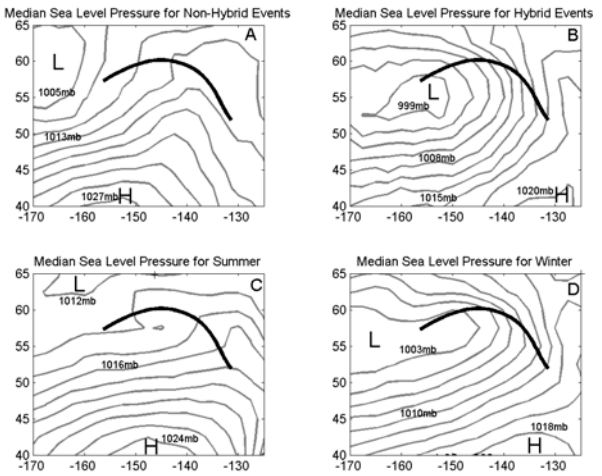


*Figure 9. Median Sea-level pressure field in Gulf of Alaska for non-hybrid events (A), hybrid events (B), summer (C), and winter (D).*

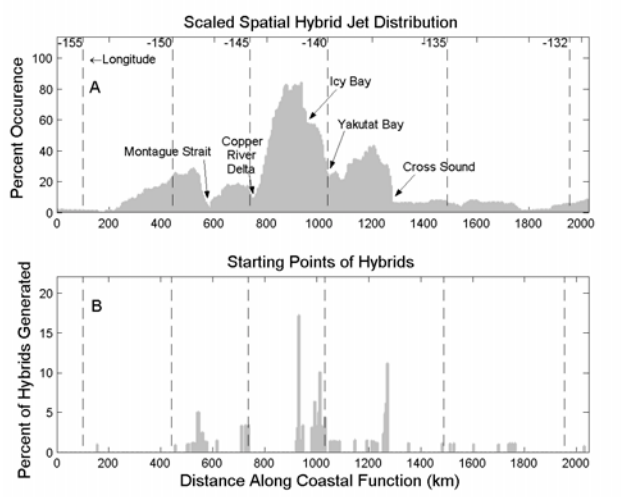


*Figure 10. Hybrid distribution as function of distance along coastal function (A). Starting points of hybrids shown in B.*

## 5. STRUCTURAL PROPERTIES

Perhaps the most important barrier jet property is its strength. The distribution of the maximum wind speeds for all barrier and hybrid jet cases (Fig. 11) reveals that a large percentage (18% for barrier and 22% for hybrid), of jets exceed the SAR saturation threshold of 25 m $s^{-1}$. The median strength of both barrier and hybrid jets is 20 m $s^{-1}$ meaning that half of the jets observed contained fairly dangerous winds. For both barrier and hybrid jets, the monthly median jet strengths (not shown) tend to be higher in the winter months. The number of jets with maximum wind speeds greater than 25 m $s^{-1}$ is much larger in the winter months as well. In fact, 92% of all barrier jets stronger than 25 m $s^{-1}$ occurred during the winter.

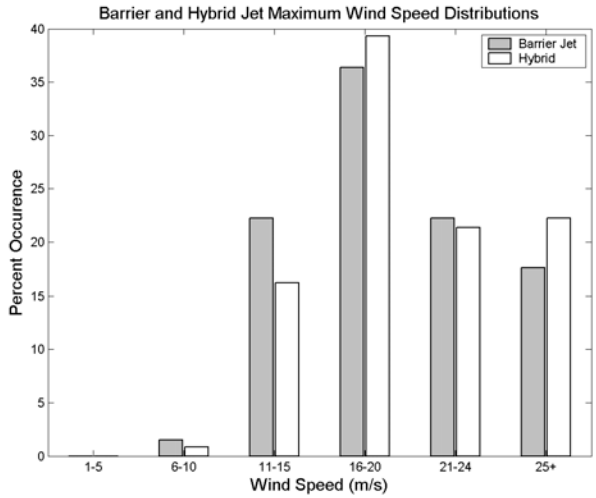


*Figure 11. Barrier and hybrid jet wind speed distributions in 5 m s-1 bins*

The median width of the barrier jets (Fig. 12) was found to be around 50 km. This value matches well with a typical Rossby radius of 100 km calculated using N = 0.01 $s^{-1}$, and terrain height of 1000 m, and f = $10^{-4}$ $s^{-1}$. The median width for hybrid jets was slightly larger (near 60 km), but very few hybrids were observed to have widths greater than 100 km.

While the median barrier jet width did not vary widely by month, the barrier jets with widths greater than 100 km were more likely to be found in the winter months. Hybrid width is more seasonally dependent than is barrier jet width. Widths tend to be greater in the winter months, and hybrids with widths greater than 100 km were never seen in the summer months (April – Aug).

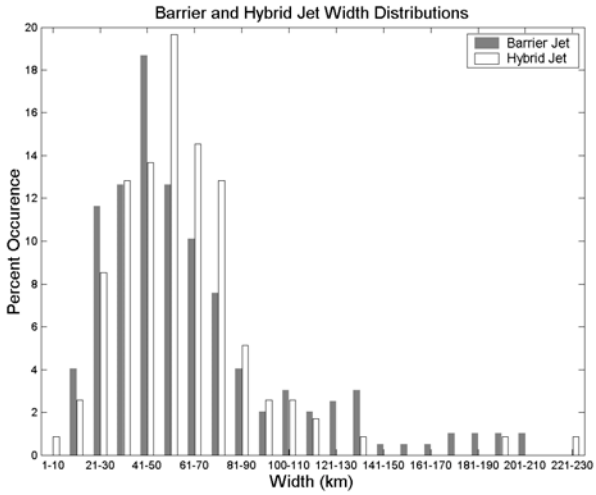


*Figure 12. Barrier jet and hybrid width distributions in 10 km bins.*

## 6. CONCLUSIONS

Coastal barrier jets in the Gulf of Alaska are more commonly found in the winter months than in summer. This wintertime maximum in barrier jet formation may be partially the result of near-shore regions of high stability in the 925-850 mb layer. Wind directions favorable for barrier jet formation show a slight seasonal cycle with the favored wind directions occurring more often during the winter. The favored locations of barrier jet formation appear to be associated with high terrain within 100 km the coast. This proximity threshold is linked to the radius of deformation distribution and that of barrier jet width, with the combined average distance inland and observed width offshore closely approximating the typical radius of deformation. Another factor influencing barrier jet formation is the dominant synoptic wind direction in the Gulf of Alaska which favors jet formation on the north and east coasts of the Gulf.

Hybrid jet formation is almost exclusively observed in the winter months and results from the much greater offshore directed pressure gradients found in this season. Each distinct maxima in the hybrid spatial distribution is linked to a gap in the coastal terrain.

Many of the observed barrier jets were quite strong with winds in excess of 25 m $s^{-1}$, with most of those occurring in the winter months.

*Acknowledgements*: This work was supported by grant ATM-0240269 from the National Science Foundation and benefited from valuable discussions with Peter Olsson of the Alaska Experimental Forecast Facility.

## 7. REFERENCES

Bell, G.D., and L.F. Bosart, 1988: Appalachian cold-air damming. *Mon. Wea. Rev.,* **116**, 137-161.

Burger, A.P., 1991: The potential vorticity equation: From planetary to small scale. *Tellus*, **43**, 191-197.

Chen, W., and R.D. Smith, 1987: Blocking and deflection of airflow by the Alps. *Mon. Wea. Rev*., **115**, 2578-2597.

Doyle, J.D., 1997: The influence of mesoscale orography on a coastal jet and rainband. *Mon. Wea. Rev*., **125**, 1465-1488.

Li, J., and Y. Chen, 1998: Barrier jets during TAMEX. *Mon. Wea. Rev.*, **126**, 959-971.

Li, X., Pichel, W., Monaldo, F., Wackerman, C., Beal, B., Clemente-Colon, P., and K, Friedman, 1999: Retrieval and validation of sea surface winds from calibrated RADARSAT ScanSAR images. Committee on Earth Observing Satellites.

Marwitz, J.D., 1987: Deep orographic storms over the Sierra Nevada. Part I: Thermodynamic and kinematic structure. *J. Atmos. Sci*., **44**, 159-173.

Marwitz, J.D., and J. Toth, 1993: The Front Range blizzard of 1990. Part I: Synoptic and mesoscale structure. *Mon. Wea. Rev*., **121**, 402-415.

Monaldo, F., 2000: The Alaska SAR demonstration and near-real-time synthetic aperture radar winds. *Johns Hopkins APL Tech. Digest*, **21**, 75-79.

Overland, J.E., and N. Bond, 1993: The influence of coastal orography: The Yakutat Storm. *Mon. Wea. Rev*., **121**, 1388-1397.

Parish, T.R., 1982: Barrier winds along the Sierra Nevada mountains. *J. Appl. Meteor.*, **21**, 925-930.

Pichel, W.G., and P. Clemente-Colon, 2000: NOAA CoastWatch SAR applications and demonstration. *Johns Hopkins APL Tech.. Digest*, **21**, 49-57.

Pierrehumbert, R.T., and B. Wyman, 1985: Upstream effects of mesoscale mountains. *J. Atmos. Sci*., **42**, 977-1003.

Schwerdtfeger, W., 1975: The effect of the Antarctic Peninsula on the temperature regime of the Weddel Sea. *Mon. Wea. Rev*., **103**, 45-51.

Schwerdtfeger, W., 1974: Mountain barrier effect on the flow of stable air north of the Brooks Range. *Proc. 24th Alaskan Science Conference*, Fairbanks, August 1973.